Dose-Response:
An International Journal
October-December 2019:1-10

DOI: 10.1177/1559325819889508
journals.sagepub.com/home/dos
SAGE

Proteomic Analysis of Radiation-Induced Acute Liver Damage in a Rabbit Model

Lingong Jiang[1], Huimin Jia[2], Zhicheng Tang[2], Xiaofei Zhu[1], Yangsen Cao[1], Yin Tang[1], Haiyan Yu[1], Jianping Cao[2], Huojun Zhang[1], and Shuyu Zhang[2,3,4]

Abstract

Radiation-induced liver damage (RILD) has become a limitation in radiotherapy for hepatocellular carcinoma. We established a rabbit model of RILD by CyberKnife. Electron microscopy analysis revealed obvious nuclear atrophy and disposition of fat in the nucleus after irradiation. We then utilized a mass spectrometry-based label-free relative quantitative proteomics approach to compare global proteomic changes of rabbit liver in response to radiation. In total, 2365 proteins were identified, including 338 proteins that were significantly dysregulated between irradiated and nonirradiated liver tissues. These differentially expressed proteins included USP47, POLR2A, CSTB, MCFD2, and CSNK2A1. Real-time polymerase chain reaction confirmed that *USP47* and *CABLES1* transcripts were significantly higher in irradiated liver tissues, whereas *MCFD2* and *CSNK2A1* expressions were significantly reduced. In Clusters of Orthologous Groups of proteins analysis, differentially expressed proteins were annotated and divided into 24 categories, including posttranslational modification, protein turnover, and chaperones. Kyoto Encyclopedia of Genes and Genomes analysis revealed that the enriched pathways in dysregulated proteins included the vascular endothelial growth factors (VEGF) signaling pathway, the mitogen-activated protein kinase (MAPK) signaling pathway, and the adipocytokine signaling pathway. The identification of proteins and pathways is crucial toward elucidating the radiation response process of the liver, which may facilitate the discovery of novel therapeutic targets.

Keywords

radiation, radiation-induced liver damage, label-free quantitative proteomics, animal model

Introduction

Radiation therapy has become a successful treatment regimen for many patients with cancer.[1,2] Technological improvements have reduced the risk of radiation-induced normal tissue damage; however, toxicity resulting in treatment breaks or long-term side effects continues to occur in a subset of patients. Ionizing radiation may significantly damage liver structure and profoundly impair its function.[3,4] Radiation-induced liver damage (RILD) has been a limitation for the radiotherapy of hepatocellular carcinoma.[3,5] In addition, radioactive materials released from nuclear accidents, wars, and other sources remain a potential threat for RILD.[6] Patients having radiogenic liver damage present with fatigue, weight gain, hepatomegaly, and anicteric ascites.[7]

In response to RILD, serum glucose, amino acids, nucleotide metabolites, and microRNAs (miRNAs) have been reported to be dysregulated.[8,9] However, there are currently no validated clinical biomarkers for the early detection of liver toxicity induced by radiation.[10] The molecular events that

[1] Department of Radiation Oncology, Shanghai Changhai Hospital, Naval Medical University, Shanghai, China
[2] School of Radiation Medicine and Protection and State Key Laboratory of Radiation Medicine and Protection, Medical College of Soochow University, Suzhou, China
[3] West China School of Basic Medical Sciences and Forensic Medicine, Sichuan University, Chengdu, China
[4] Second Affiliated Hospital of Chengdu Medical College (China National Nuclear Corporation 416 Hospital), Chengdu, China

Received 01 May 2019; received revised 07 October 2019; accepted 08 October 2019

Corresponding Authors:
Huojun Zhang, Department of Radiation Oncology, Shanghai Changhai Hospital, the Naval Medical University, No. 168 Changhai Road, Shanghai 200433, China.
Email: chyyzhj@163.com

Shuyu Zhang, Second Affiliated Hospital of Chengdu Medical College (China National Nuclear Corporation 416 Hospital), Chengdu 610051, China.
Email: zhang.shuyu@hotmail.com

participate in normal tissue damage are complex, including oxidative stress, inflammation, depletion of injured cells, senescence, and cytokines. Numerous studies have identified various cytokines leading to the progression of RILD. These cytokines include interleukin-1β, transforming growth factor β (TGF-β), tumor necrosis factor α, and interleukin 10.[11] Smad3 is a mediator of the fibrotic response to TGF-β pathway.[12] Intervention against TGF-β was found to halt the progression of established radiation-induced liver fibrosis.[13] Moreover, hepatocyte growth factor electrogene therapy would protect the liver from RILD by preventing apoptosis and downregulation of TGF-β.[14]

Currently, the pathogenesis of acute RILD remains unclear. Therefore, understanding the molecular alterations, regulatory networks, signaling cascades, and metabolic pathways that occur during RILD will contribute to the therapeutic targets for this disease. Many novel approaches have been introduced to identify key regulators associated with disease progression. It was reported that RNA sequencing had been employed to identify miRNA profiles of RILD in a mouse model.[15]

Proteomic profiling is one of the most commonly applied strategies for protein discovery.[16,17] An investigation into the differential proteome expression patterns of liver tissue upon exposure to radiation may contribute toward a better understanding of its pathogenesis and adaptive response. Here, we utilized a mass spectrometry-based label-free relative quantitative proteomics approach to investigate and compare global proteomic changes of rabbit liver in response to radiation.

Materials and Methods

Liver Irradiation of Rabbits

Twenty adult male New Zealand white rabbits were purchased from the Shanghai SLAC Laboratory Animal Co, Ltd (Shanghai, China). The rabbits were shaved in the upper right quadrant of the abdomen, and the skin was disinfected. A fiducial, which was regarded as a reference for target delineation, was implanted in the external part of the right liver lobe guided by ultrasound (Prosound F75; Hitachi Aloka Medical Ltd, Mure, Mitaka-Shi, Tokyo, Japan). General anesthesia was performed before fiducial implantation. When the needle was inserted at the potential implantation area, the fiducial was pushed through the needle into the area. A computed tomography (CT; Philips Medical Systems, Best, North Brabant, the Netherlands) scan was performed 1 week later to determine whether there was displacement of the fiducial before CT simulation. The plain and enhanced CT scan images were transferred to the CyberKnife MultiPlan system (Accuray Incorporated, Sunnyvale, California). The organs at risk (OARs) and the gross tumor volume (GTV) were delineated on the registered images. The GTV was defined as the hepatic tissues around the fiducial, in the shape of a sphere with a radius of approximately 1 cm. The maximum cross-section of the sphere was parallel to the axial plane of the fiducial. After contouring the OARs and target volumes, the treatment plan was optimized based on dose constraints and other parameters. The radiation dose to the target volume was 20 Gy/fraction. The target volume was tracked by the XSight Spine and Synchrony Tracking technique. Radiotherapy was delivered via CyberKnife (Accuray Incorporated). The rabbits were killed 3 days after irradiation. The exterior portion of the right lobe (irradiated area) and the exterior portion of the left lobe (nonirradiated area) of each rabbit's liver were removed to perform follow-up experiments. Protocols for experiments involving animals were approved by the Animal Experimentation Ethics Committee at Shanghai Changhai Hospital, the Naval Medical University (Shanghai, China).

Transmission Electron Microscopy

Liver tissues were fixed for 2 hours with 2.5% glutaraldehyde in 0.05 M/L sodium cacodylate buffer (pH 7.2) at room temperature, followed by 2 hours in 2% osmium tetroxide in 0.1 M/L sodium cacodylate buffer and 18 hours in 1% aqueous uranyl acetate. After dehydration through an ethanol series, the specimens were embedded in Epon 812, and ultrathin sections were collected on copper grids. After being stained with uranyl acetate and lead citrate, the sections were examined using a Tecnai G2 Spirit BioTwin transmission electron microscope (FEI Company, Hillsboro, Oregon).

Gel Electrophoresis

Each group (nonirradiated and irradiated groups) consisted of 3 tissue samples from 3 rabbits. Sodium dodecyl sulfate polyacrylamide gel electrophoresis (PAGE) was performed using NuPAGE 4% to 12% Bis-Tris gels (Cambridge, Massachusetts). Electrophoresis of the liver tissue samples was performed at a constant current of 120 mA for 1 hour. Then the gel was fixed with a solution of 50% methanol and 10% acetic acid for 1 hour and stained overnight with 0.1% Coomassie Brilliant Blue in 50% methanol and 10% acetic acid. The gel was subsequently destained with distilled water, followed by the 50% methanol and 10% acetic acid solution until the background was clear. Each PAGE lane was cut into 15 slices for in-gel digestion.

Sample Preparation

Briefly, the samples were first denatured in 8 mol/L urea, disulfide linkages were reduced with dithiothreitol, and all cysteine residues were alkylated with iodoacetamide. The samples were then cleaned using a C18-based spin column (Pep-Clean C18 Spin Columns; Thermo Fisher, Santa Clara, California) and digested with sequencing-grade modified trypsin in digestion buffer (ammonium bicarbonate 100 mmol/L, pH 8.5). The peptides obtained through digestion were completely dried down in a SpeedVac device (Thermo Fisher, Woburn, Massachusetts). The dried sample was redissolved in sample solution (2% acetonitrile, 97.5% water, and 0.5% formic acid). Finally, the dissolved peptide samples were analyzed using a Nano Liquid chromatography electrospray ionisation tandem mass spectrometry (LC-ESI-MS/MS) system.

Table 1. Primer Sequences for Real-Time PCR Analysis.

Gene	Forward Primer	Reverse Primer
USP47	ATACTGCTGATATGGCTTCACTGG	TGTCATCCACGGCATTAGAATCC
CABLES1	ATCATTGGTCTTGAAGGTGTGGAG	GGAGGAGGCGGAGTCTATGG
CSNK2A1	CGCCAATATGATGTCAGGGATTTC	CAGAGGTCCGAGAGGTGAAGG
MCFD2	TCTCCACCGCCATCACTCAC	TGCCTGTTCACTCCCTTCCTC

Abbreviation: PCR, polymerase chain reaction.

NanoLC-ESI-MS/MS Analysis

NanoLC-ESI-MS/MS analysis of the digested protein samples was carried out using a high-performance liquid chromatography (HPLC) system (Agilent, Santa Clara, California) with a reverse-phase C18 column, 8 cm in length with a 75 μm inner diameter. The particle size of the C18 column was 3 μm, with a pore size of 300 Å, and the injection time was 20 minutes; HPLC solvent A consisted of 97.5% water, 2% acetonitrile, and 0.5% formic acid, and HPLC solvent B consisted of 9.5% water, 90% acetonitrile, and 0.5% formic acid. The gradient time was 60 minutes from 2% solvent B to 90% solvent B, plus 20 minutes for sample loading and 20 minutes for column washing. The column flow rate was approximately 800 nL per minute after splitting, with a typical injection volume of 3 μL.

The HPLC system was online coupled to an ion trap mass spectrometer (LCQ DECA XP PLUS; Thermo Fisher) in a manner such that a sample eluted from the HPLC column was directly ionized through an electrospray ionization process and entered the mass spectrometer. The mass spectrometer was set to data-dependent mode to acquire MS/MS data via a low-energy collision-induced dissociation process. One full scan with 1 microscan in the mass range of 550 to 1800 amu was acquired, followed by 1 MS/MS scan of the most intense ion with a full mass range and 3 microscans. The exclusion width was 4 Da.

Database Search and Validation

The mass spectrometry data were employed in searches against the most recent nonredundant protein database (National Center for Biotechnology Information) with ProtTech's ProtQuest software suite. The output from the database searches was manually validated by a senior scientist before reporting.

Label-Free Protein Quantitation

The scoring function was based on the MS abundance recorded in both the MS and MS/MS data sets, spectral count (number of MS/MS spectra per peptide), unique peptide numbers, and fragmentation (MS/MS) intensities. The normalized spectral index (SIN) was calculated for each gel slice based on the correlation equation. The final relative protein abundance was the percentage of each SIN in the total SIN in each sample.

Bioinformatic Analysis of Proteomic Data

We analyzed all of the dysregulated proteins using Kyoto Encyclopedia of Genes and Genomes (KEGG) pathway analysis and the DAVID 6.8 database (http://david.ncifcrf.gov/). Clusters of Orthologous Group (COG) analysis of DEPs was also employed for functional annotation.[18]

Protein–Protein Interaction Network Construction

Cytoscape (version 3.2.0)[19] was utilized to construct a protein–protein interaction (PPI) network, and the degree centrality of topology property was applied to estimate the score of a node in the network. A higher scoring node indicated a more potential hub gene.

RNA Extraction and Real-Time Polymerase Chain Reaction Analysis

Total RNA from liver tissues was extracted with TRIzol (Invitrogen, Carlsbad, California) and reverse transcribed to complementary DNA (cDNA) using an oligo$(dT)_{12}$ primer and Superscript II (Invitrogen). The SYBR green dye (Takara, Japan) was used for amplification of cDNA. Messenger RNA levels and levels of the internal standard *glyceraldehyde 3-phosphate dehydrogenase* were measured by real-time quantitative polymerase chain reaction (PCR) in triplicate using a Prism 7900 real-time PCR machine (Applied Biosystems, Foster City, California). The primers are listed in Table 1.

Statistical Analysis

Data were shown with the mean $\pm$ standard error of the mean of at least 3 independent experiments. One-way analysis of variance was employed to determine statistical significance. The statistical analyses were performed using IBM SPSS Statistics 20.0 software (IBM SPSS Inc, Somers, New York). Differences were considered significant at $P < .05$.

Results

Radiation-Induced Liver Damage in a Rabbit Model

We first established RILD in a rabbit model using a single dose of 20 Gy with high-precision-focused irradiation by fiducial implantation. No hemorrhage or other complications occurred in all rabbits during the implantation of fiducials (Figure 1A

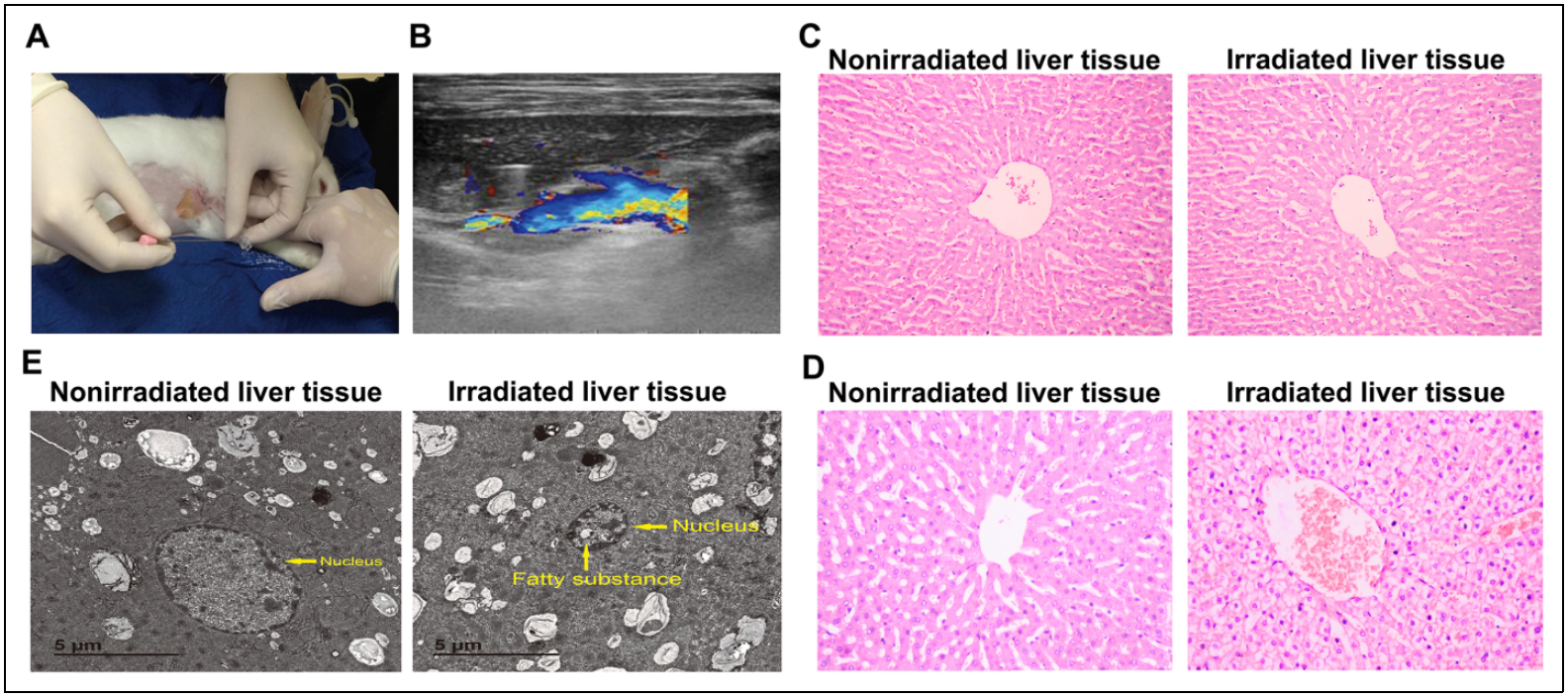

Figure 1. Radiation disrupted the subcellular structure of liver cells. (A) The fiducial is placed into the needle sheath and will be pushed into the liver by a puncture needle. (B) On color Doppler flow imaging, a fine needle–like dense echo strip (fiducial sonogram) and posterior comet tail sign can be seen, and the sonogram does not move with the change of body position. The fiducial implantation point has a certain distance from the large blood vessel. (C) H&E staining of irradiated and nonirradiated liver tissues of rabbits 3 days after radiation. (D) H&E staining of irradiated and nonirradiated liver tissues of rabbits 14 days after radiation. (E) Electron microscopy analysis of irradiated and nonirradiated liver tissues of rabbits (magnification: ×2000).

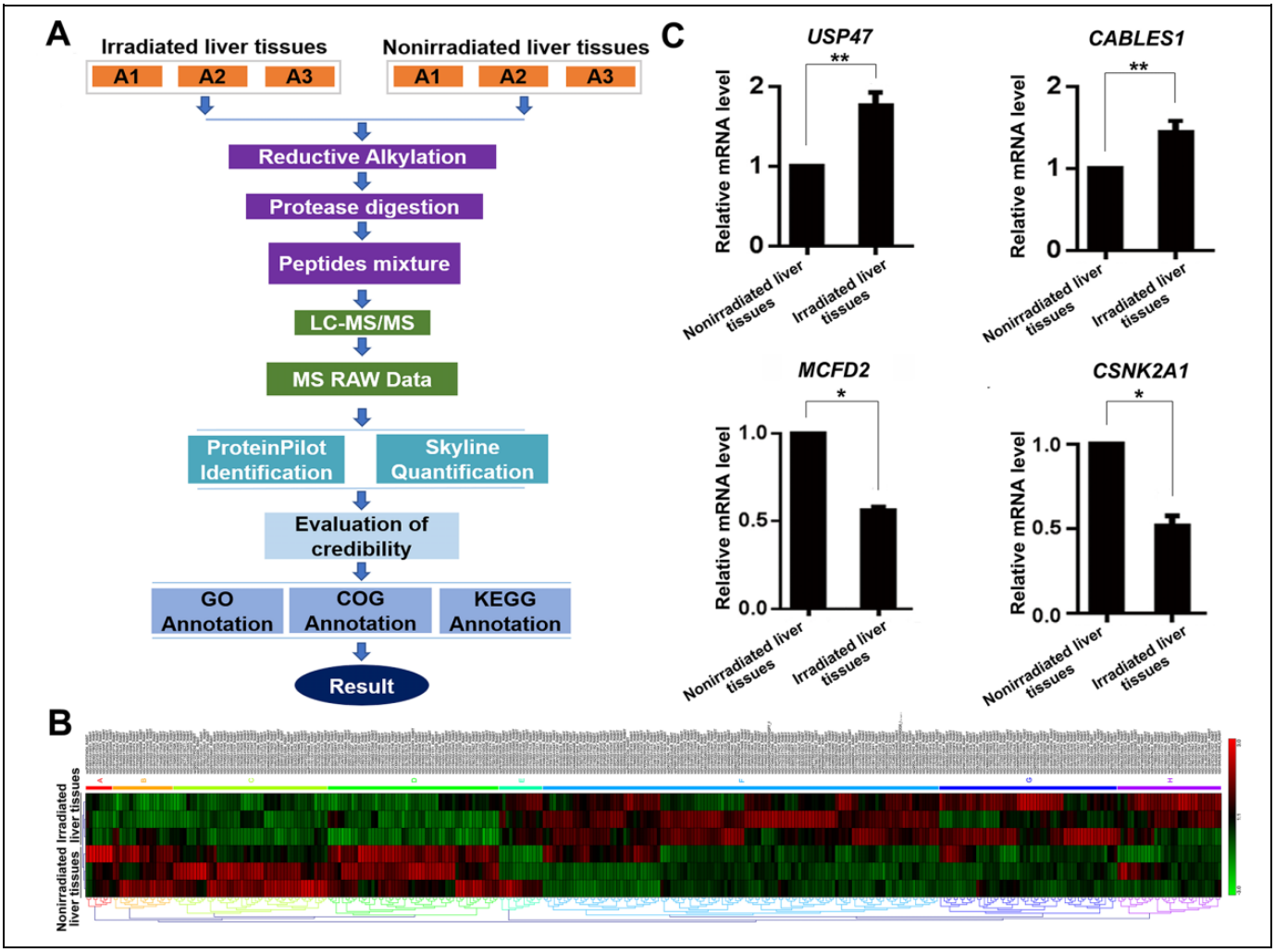

Figure 2. Proteomic analysis of dysregulated proteins between irradiated and nonirradiated liver tissues of rabbits. (A) Experimental design of the proteomic analysis. (B) Heatmap of dysregulation in irradiated liver tissues. Proteins were identified by label-free quantitative proteomic analysis. (C) Real-time PCR analysis of mRNAs. Relative mRNA levels of *USP47*, *CABLES1*, *MCFD2*, and *CSNK2A1* were normalized to *glyceraldehyde 3-phosphate dehydrogenase*. *$P < .05$; **$P < .01$. mRNA indicates messenger RNA; PCR, polymerase chain reaction.

and B). During the period of irradiation to execution, there were no significant changes regarding weight, vitality, or food consumption, and no radiation-induced dermatitis was seen. When the rabbits were killed and dissected on the third day after irradiation, the color of the irradiated liver tissues and the nonirradiated liver tissues was a normal reddish brown color, and no obvious signs of congestion were found (Figure 1C). Under electron microscopy, an obvious atrophy of the nucleus and disposition of fat in the nucleus in the irradiated area was revealed, and the outline of mitochondria and endoplasmic reticulum is unclear (Figure 1E). Correspondingly, the rabbits were killed 2 weeks later and the hepatic cord showed disorderly arrangement, with narrowed sinusoids, dilated and slightly congested central veins of lobules, liver cell edema, and partial fatty degeneration (Figure 1D). The above results indicated that acute RILD occurred in this rabbit model.

Proteins Were Dysregulated in Radiation-Induced Rabbit Liver

We next investigated the proteomic profiles of the irradiated liver tissues and corresponding nonirradiated liver tissues by label-free quantitative proteomic analysis. A total of 18 256 peptides, which match 2365 proteins, were successfully identified. Screening by $P < .05$ and fold change >2.0, a total of 338 significantly dysregulated proteins were identified between irradiated and nonirradiated liver tissues. Among these proteins, there were 217 overexpressed and 121 underexpressed proteins in the irradiated liver tissues compared with the corresponding normal liver tissues (Figure 2B and Supplementary Table 1). The identified differentially expressed proteins (DEPs) included USP47, POLR2A, CSTB, CABLES1, MCFD2, CAP1, and CSNK2A1.

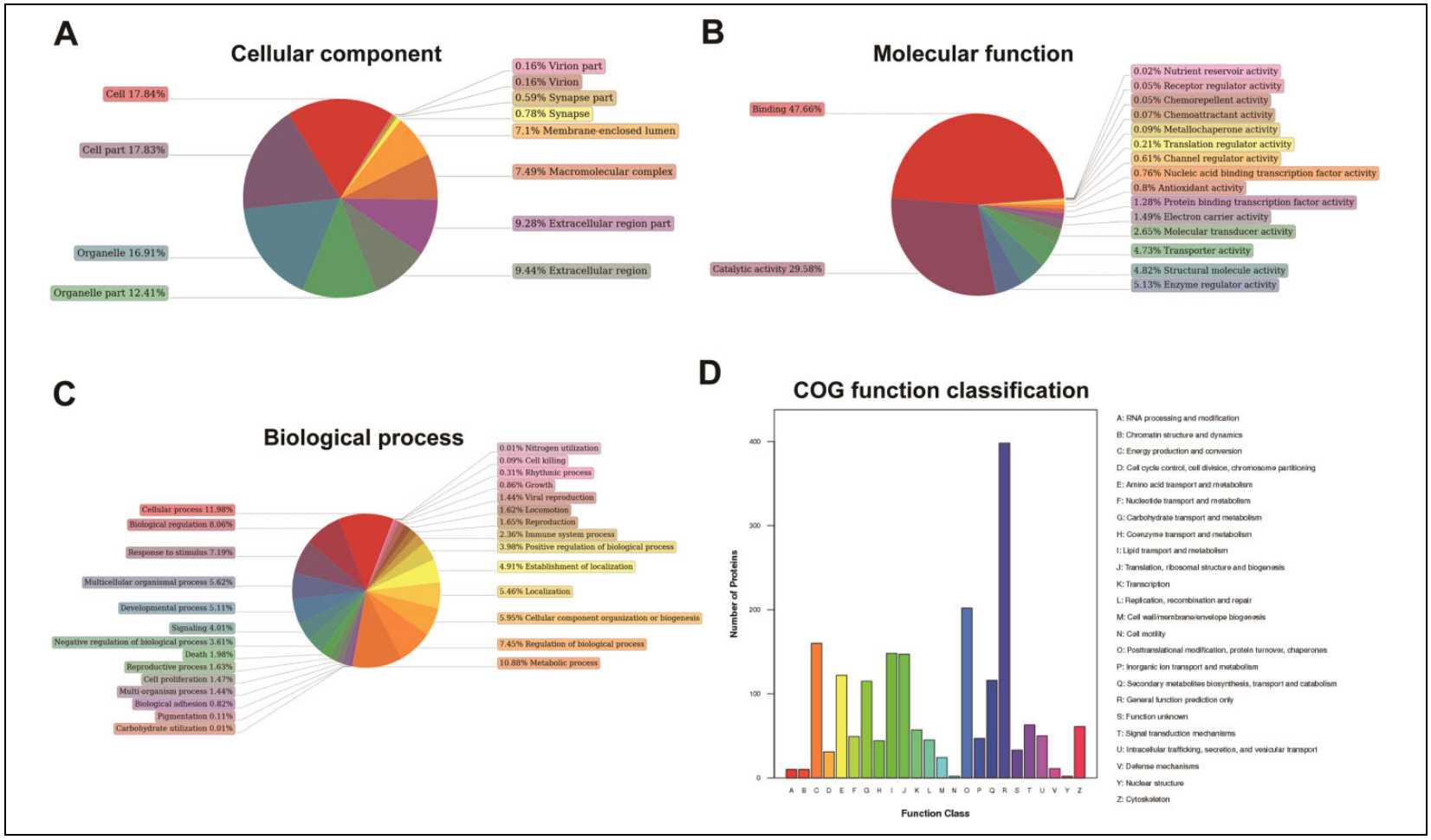

Figure 3. Gene Ontology and COG analyses of the dysregulated proteins between irradiated and nonirradiated liver tissues of rabbits. (A) The subcellular location of up- and downregulated proteins (irradiated tissues vs control nonirradiated tissues). (B) Molecular function enrichment analysis of up- and downregulated proteins. (C) Biological process enrichment analysis of up- and downregulated proteins. (D) The COG pathway enrichment analysis of up- and downregulated proteins. COG indicates Clusters of Orthologous Group.

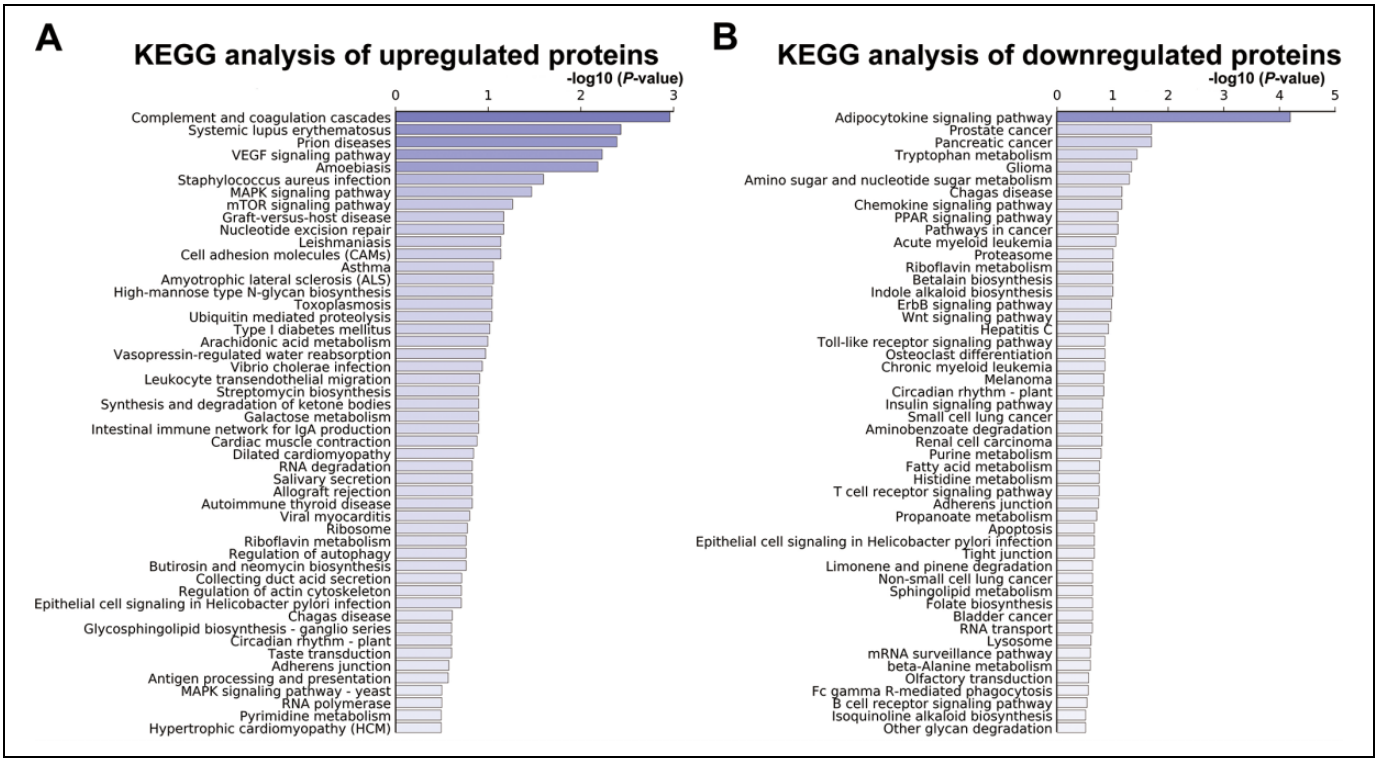

Figure 4. The KEGG analysis of the dysregulated proteins. The KEGG pathway enrichment analysis of (A) upregulated and (B) downregulated proteins. KEGG indicates Kyoto Encyclopedia of Genes and Genomes.

We next validated the expression of the dysregulated genes using real-time PCR. The results showed that *USP47* and *CABLES1* transcripts were significantly higher in irradiated liver tissues, whereas *MCFD2* and *CSNK2A1* expressions were significantly reduced (Figure 2C). These results were consistent with the results from proteomic analysis.

Functional Annotation of DEPs

All of the DEPs were assigned into functional groups according to Gene Ontology analysis. In the cellular component ontology, the dominant groups were "cell," "cell parts" and "organelle," and "organelle part" (Figure 3A). Meanwhile, in the molecular function ontology, the dominant groups were "binding" and "catalytic activity" (Figure 3B). In the biological process ontology, the most dominant groups were "cellular process," "metabolic process," and "biological regulation" (Figure 3C). The cellular component and molecular function ontology analysis also convinced us that the DEPs mainly functioned within the cell.

In COG analysis, DEPs were annotated and divided into 24 categories (Figure 3D), showing differences in functional annotation between irradiated and nonirradiated liver tissues. The significantly dominant group of preferentially expressed proteins was "posttranslational modification," "protein turnover and chaperones," "energy production and conversion," and "lipid transport and metabolism." The enrichment of gene functional annotation suggested high-protein posttranslational processing and high-energy requirements in response to radiation in the liver.

The KEGG pathway analysis was performed to investigate pathways that may be involved in RILD. The enriched pathways in upregulated proteins included complement and coagulation cascades, the vascular endothelial growth factors (VEGF) signaling pathway, and the mitogen-activated protein kinase (MAPK) signaling pathway (Figure 4A). The pathways associated with downregulated proteins included the adipocytokine signaling pathway, cancer pathways, and tryptophan metabolism (Figure 4B). A PPI network was established by PPI software. As shown in Figure 5, there were 167 nodes showing 418 potential PPIs between the dysregulated proteins.

Discussion

Radiation-induced liver damage usually accompanies radiotherapy of hepatocellular carcinoma, which often manifests as subacute and chronic liver damage in clinic.[20,21] Although studies on RILD have been ongoing for decades, the molecular pathogenesis remains unclear. At present, there is still no effective treatment for this disease.[22] Radiation-induced liver damage severely restricts the increase of the tumor radiotherapy dose and the reirradiation of hepatobiliary tumors.[23] The irradiation techniques used in previous reports were mostly 2-dimensional block or 3-dimensional conformal, and almost all of the liver is irradiated,[24,25] which makes it difficult to compare irradiated and nonirradiated areas in 1 animal. Limitations

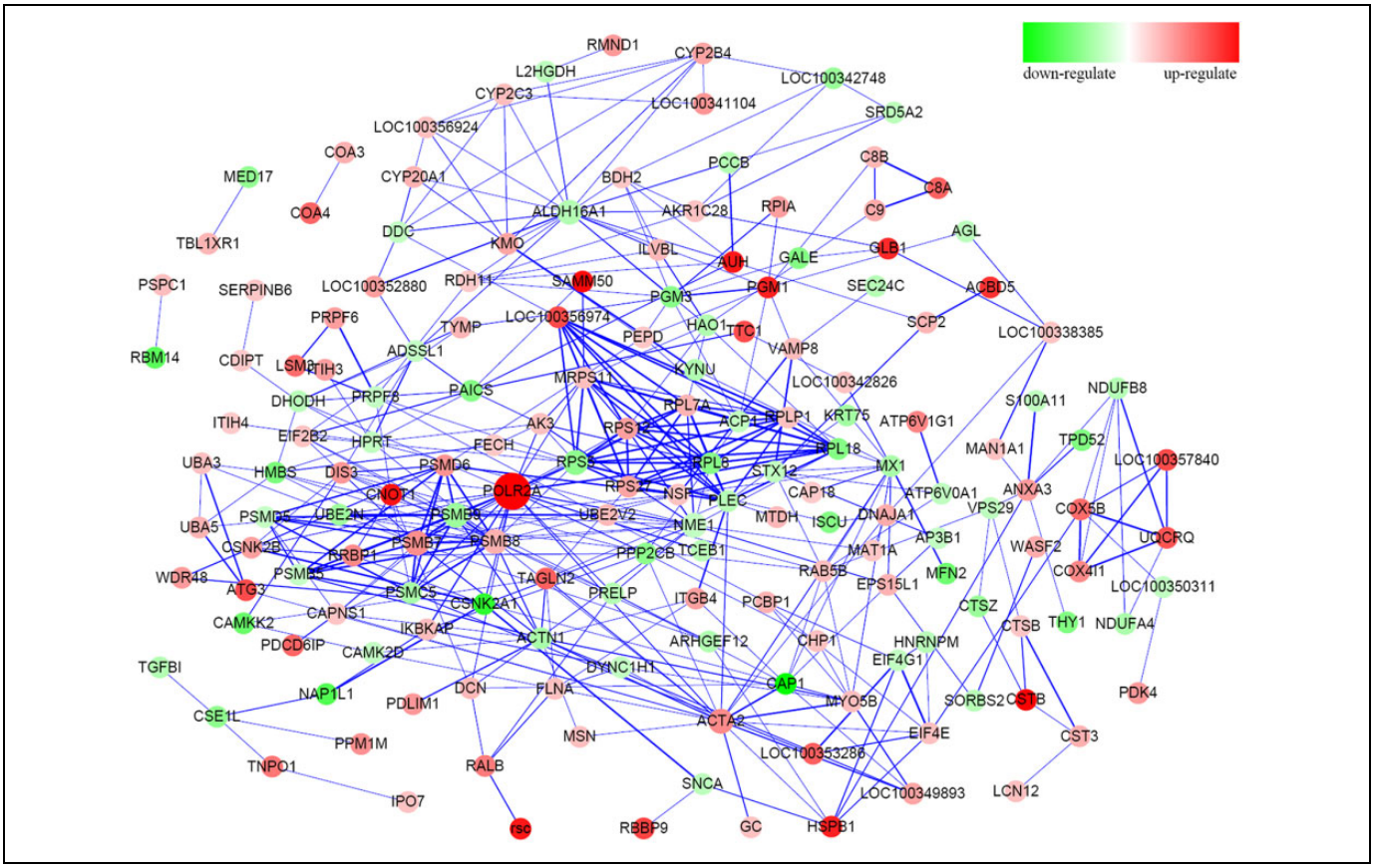

Figure 5. Protein–protein interaction network of the dysregulated proteins. Protein–protein interaction network and significant clustered module of differentially expressed proteins. Red circles represent the upregulated genes, and green circles represent downregulated genes. Larger node sizes indicate more higher node degrees.

of irradiation technology, and liver movement due to diaphragmatic movement and gastrointestinal motility, easily lead to poor irradiation accuracy. In this experiment, we chose a single dose of 20 Gy to irradiate the liver by CyberKnife in order to establish a rabbit model of acute RILD. CyberKnife, with a focused stereotactic precision irradiation technique, was used to perform partial liver lobe irradiation, which has been widely utilized in clinical stereotactic radiotherapy for liver cancer.[26] To further improve the radiation accuracy, we implanted a fiducial into the exterior portion of the right lobe of the rabbit liver through ultrasound guidance, so that the irradiation error could be controlled within 0.5 mm.

Proteomics is a powerful tool that has been widely used to identify new unannotated and aberrantly expressed proteins in diseases.[27] This study is the first report to describe the changes in protein expression in acute rabbit RILD, providing insight into the molecular pathogenesis of this disease. In total, 2365 proteins were successfully identified, including 338 proteins that were significantly dysregulated between irradiated and nonirradiated liver tissues. The identification of proteins is crucial toward elucidating the radiation response process of the liver, which may facilitate the discovery of novel therapeutic targets and effective radioprotectors. We believe that some differential proteins screened in this study can be activated or inhibited to alleviate RILD in patients with hepatocellular carcinoma. For example, USP47, a differential protein in this study, is a deubiquitinase, has been reported to regulate β-catenin ubiquitination, and plays a positive role in regulating Wnt target gene expression.[28] The canonical Wnt/β-catenin pathway stimulates fibroblast accumulation and myofibroblast differentiation, which promotes radiation-induced fibrosis.[29] In addition, USP47 acts posttranslationally to counteract a proteasome-mediated event that reduces MAPK half-life and thereby dampens signaling output.[30] MAPK, classified as a stress-activated kinase, maintains hepatocyte cell cycle arrest in the adult liver. Its inactivation plays an important role in liver regeneration.[31] Cyclase-associated protein 1 (CAP1), a downregulated protein, has been shown to regulate cell proliferation in cancer cells as well as noncancerous cells.[32,33] Reduced expression of CAP1 may inhibit the recovery from liver damage by radiation and represent a therapeutic target. The roles of the dysregulated proteins warrant further investigation.

Bakshi et al investigated proteomic expression after low-dose irradiation (0.02-1.0 Gy) using neonatal mice.[34] They found significant changes in liver metabolism, including the glycolysis pathway, pyruvate dehydrogenase availability, and lipid metabolism. Consistently, we also found dysregulated

lipid metabolism and energy supply pathways in irradiated liver tissues by COG analysis. Chung et al reported identified proteins of radiation-induced hepatic toxicity in cirrhotic rats using 2-dimensional electrophoresis and quadrupole time-of-flight mass spectrometry.[35] They found 20 dysregulated proteins including CTNNA1, tuberin, HGFR, and metallothionein 1. However, the dysregulated proteins in our study differ from the above reports, indicating that the high dose of radiation resulted in different network responses compared to normal liver. Besides, in our research, the VEGF signaling pathway was involved in upregulated proteins. This pathway has been shown to attenuate liver injury[27] and to promote liver fibrosis.[36] The secretion of adipocytokines has been reported to regulate the progression of liver diseases.[37,38] These pathways provide novel intervention strategies against RILD.

Potential limitations of this study include: (1) ultrasound-guided fiducial implantation is a minimally invasive procedure, which requires careful techniques; and (2) we only studied the radiation damage of liver tissue in normal rabbits, lacked the study of tumor-bearing rabbits, and model with basic liver diseases. Therefore, we will carry out relevant research in the future.

In summary, we identified 338 preferentially expressed proteins and multiple pathways induced by irradiation in rabbits' liver tissue. Our results provide a better understanding of the global proteomic alterations of the liver in response to radiation, which may contribute to diagnostic and therapeutic targets.

Authors' Note

Lingong Jiang and Huimin Jia contributed equally to this work.

Declaration of Conflicting Interests

The author(s) declared no potential conflicts of interest with respect to the research, authorship, and/or publication of this article.

Funding

The author(s) disclosed receipt of the following financial support for the research, authorship, and/or publication of this article: This work is supported by the National Natural Science Foundation of China (grant number 31770911, 81673100 and 81872453), Social Development Program of Jiangsu Province (grant number BE2017652), Key Scientific Development Program of China (grant number 2016YFC0904700 and 2016YFC0904702), Science and Technology Commission of Shanghai Municipality (grant number 18ZR1438700), and China Health Promotion Foundation (grant number THC2015001).

ORCID iD

Lingong Jiang https://orcid.org/0000-0002-6214-2069
Shuyu Zhang https://orcid.org/0000-0003-1419-3635

Supplemental Material

Supplemental material for this article is available online.

References

1. Thariat J, Hannoun-Levi JM, Sun Myint A, Vuong T, Gérard JP. Past, present, and future of radiotherapy for the benefit of patients. *Nat Rev Clin Oncol*. 2013;10(1):52-60.
2. Toya R, Saito T, Kai Y, et al. Impact of (99 m)Tc-GSA SPECT image-guided inverse planning on dose-function histogram parameters for stereotactic body radiation therapy planning for patients with hepatocellular carcinoma: a dosimetric comparison study. *Dose Response*. 2019;17(1):1559325819832149.
3. Lawrence TS, Robertson JM, Anscher MS, Jirtle RL, Ensminger WD, Fajardo LF. Hepatic toxicity resulting from cancer treatment. *Int J Radiat Oncol Biol Phys*. 1995;31(5):1237-1248.
4. Azizova TV, Batistatou E, Grigorieva ES, et al. An assessment of radiation-associated risks of mortality from circulatory disease in the cohorts of Mayak and Sellafield nuclear workers. *Radiat Res*. 2018;189(4):371-388.
5. Cheng JC, Wu JK, Huang CM, et al. Radiation-induced liver disease after three-dimensional conformal radiotherapy for patients with hepatocellular carcinoma: dosimetric analysis and implication. *Int J Radiat Oncol Biol Phys*. 2002;54(1):156-162.
6. Taylor DM, Taylor SK. Environmental uranium and human health. *Rev Environ Health*. 1997;12(3):147-157.
7. Guha C, Kavanagh BD. Hepatic radiation toxicity: avoidance and amelioration. *Semin Radiat Oncol*. 2011;21(4):256-263.
8. Cuneo KC, Sun Y, Schipper M, et al. MicroRNAs predict liver toxicity in patients receiving stereotactic body radiation therapy for hepatocellular carcinoma. *Int J Radiat Oncol Biol Phys*. 2016;96(2):S202-S203.
9. Kurland IJ, Broin PO, Golden A, et al. Integrative Metabolic Signatures for Hepatic Radiation Injury. *PloS One*. 2015; 10(6):e0124795.
10. Munoz-Schuffenegger P, Ng S, Dawson LA. Radiation-induced liver toxicity. *Semin Radiat Oncol*. 2017;27(4):350-357.
11. Ozyurt H, Ozden AS, Cevik O, et al. Investigation into the role of the cholinergic system in radiation-induced damage in the rat liver and ileum. *J Radiat Res*. 2014;55(5):866-875.
12. Flanders KC. Smad3 as a mediator of the fibrotic response. *Int J Exp Pathol*. 2004;85(2):47-64.
13. Du SS, Qiang M, Zeng ZC, et al. Radiation-Induced liver fibrosis is mitigated by gene therapy inhibiting transforming growth factor-β Signaling in the rat. *Int J Radiat Oncol Biol Phys*. 2010;78(5):1513-1523.
14. Chi CH, Liu IL, Lo WY, Liaw BS, Wang YS, Chi KH. Hepatocyte growth factor gene therapy prevents radiation-induced liver damage. *World J Gastroenterol*. 2005;11(10):1496-1502.
15. Lu J, Chen C, Hao L, Zheng Z, Zhang N, Wang Z. MiRNA expression profile of ionizing radiation-induced liver injury in mouse using deep sequencing. *Cell Biol Int*. 2016;40(8):873-886.
16. Cho WC. Proteomics and translational medicine: molecular biomarkers for cancer diagnosis, prognosis and prediction of therapy outcome. *Expert Rev Proteomics*. 2011;8(1):1-4.
17. Sun W, He F. Applications of proteomics in hepatic diseases research. *Sci China C Life Sci*. 2004;47(2):101-106.

18. Tatusov RL, Galperin MY, Natale DA, Koonin EV. The COG database: a tool for genome-scale analysis of protein functions and evolution. *Nucleic Acids Res*. 2000;28(1):33-36.
19. Shannon P, Markiel A, Ozier O, et al. Cytoscape: a software environment for integrated models of biomolecular interaction networks. *Genome Res*. 2003;13(11):2498-2504.
20. Peixoto A, Pereira P, Bessa de Melo R, Macedo G. Radiation-induced liver disease secondary to adjuvant therapy for extra-hepatic cholangiocarcinoma. *Dig Liver Dis*. 2017;49(2):227.
21. Pan CC, Kavanagh BD, Dawson LA, et al. Radiation-associated liver injury. *Int J Radiat Oncol Biol Phys*. 2010; 76(3):S94-100.
22. Sanuki N, Takeda A, Oku Y, et al. Influence of liver toxicities on prognosis after stereotactic body radiation therapy for hepatocellular carcinoma. *Hepatol Res*. 2015;45(5):540-547.
23. Doi H, Shiomi H, Masai N, et al. Threshold doses and prediction of visually apparent liver dysfunction after stereotactic body radiation therapy in cirrhotic and normal livers using magnetic resonance imaging. *J Radiat Res*. 2016;57(3):294-300.
24. Liu Y, Shi C, Cui M, Yang Z, Gan D, Wang Y. Different doses of partial liver irradiation promotes hepatic regeneration in rat. *Int J Clin Exp Pathol*. 2015;8(6):6554-6559.
25. Liu H, Wang S, Wu Z, et al. Glibenclamide, a diabetic drug, prevents acute radiation induced liver injury of mice via up-regulating intracellular ROS and subsequently activating Akt-NF-κB pathway. *Oncotarget*. 2017;8(25):40568-40582.
26. Song J H, Jeong B K, Choi H S, et al. Defining radiation-induced hepatic toxicity in hepatocellular carcinoma patients treated with stereotactic body radiotherapy. *J Cancer*. 2017;8(19):4155-4161.
27. Cheema AK, Byrum SD, Sharma NK, et al. Proteomic changes in mouse spleen after radiation-induced injury and its modulation by gamma-tocotrienol. *Radiat Res*. 2018;190(5):449-463.
28. Shi JD, Liu YJ, Xu XH, et al. Deubiquitinase USP47/UBP64E Regulates beta-catenin ubiquitination and degradation and plays a positive role in Wnt signaling. *Mol Cell Biol*. 2015;35(19): 3301-3311.
29. Vallée A, Lecarpentier Y, Guillevin R, Vallée JN. Interactions between TGF-β1, canonical WNT/β-catenin pathway and PPAR γ in radiation-induced fibrosis. *Oncotarget*. 2017;8(52):90579-90604.
30. Ashton-Beaucage D, Lemieux C, Udell CM, Sahmi M, Rochette S, Therrien M. The deubiquitinase USP47 stabilizes MAPK by counteracting the function of the N-end rule ligase POE/UBR4 in drosophila. *PLoS Biol*. 2016;14(8):e1002539.
31. Campbell JS, Argast GM, Yuen SY, Hayes B, Fausto N. Inactivation of p38 MAPK during liver regeneration. *Int J Biochem Cell B*. 2011; 43(2):180-188.
32. Bao Z, Qiu XJ, Wang DL, et al. High expression of adenylate cyclase-associated protein 1 accelerates the proliferation, migration and invasion of neural glioma cells. *Pathol Res Pract*. 2016; 212(4):264-273.
33. Zhang HY, Liu YH, Li Y, et al. The expression of CAP1 after traumatic brain injury and its role in astrocyte proliferation. *J Mol Neurosci*. 2014;54(4):653-663.
34. Bakshi MV, Azimzadeh O, Barjaktarovic Z, et al. Total body exposure to low-dose ionizing radiation induces long-term alterations to the liver proteome of neonatally exposed mice. *J Proteome Res*. 2015;14(1):366-373.
35. Chung SI, Seong J, Park YN, Kim WW, Oh HJ, Han KH. Identification of proteins indicating radiation-induced hepatic toxicity in cirrhotic rats. *J Radiat Res*. 2010;51(6):643-650.
36. Wynn TA. Cellular and molecular mechanisms of fibrosis. *J Pathol*. 2008;214(2):199-210.
37. Novo E, Cannito S, Patemostro C, Bocca C, Miglietta A, Parola M. Cellular and molecular mechanisms in liver fibrogenesis. *Arch Biochem Biophys*. 2014;548:20-37.
38. Parker R, Kim SJ, Gao B. Alcohol, adipose tissue and liver disease: mechanistic links and clinical considerations. *Nat Rev Gastroenterol Hepatol*. 2018;15(1):50-59.